ChemComm

COMMUNICATION

View Article Online
View Journal

Cite this: DOI: 10.1039/d2cc01434c

Received 15th March 2022,
Accepted 12th April 2022

DOI: 10.1039/d2cc01434c

rsc.li/chemcomm

Long-lived, near-IR emission from Cr(III) under ambient conditions†

Natalia Sawicka,[a] Chloe J. Craze,[a] Peter N. Horton,[b] Simon J. Coles,[b] Emma Richards *[a] and Simon J. A. Pope *[a]

Bis-terdentate (N^N^N) ligands coordinated to Cr(III) yield complexes that display near-IR emission under aerated solvent conditions at room temperature.

Cr(III) complexes have attracted interest due to their optical,[1] (photo)redox and magnetic properties.[2] Cr(III) photoluminescence,[3] from a discreet coordination complex was first reported in the 1960s.[4] The photophysics of Cr(III) complexes is generally dominated by metal-centred excited states.[5–7] A strong, pseudo-octahedral ligand field at Cr(III) yields the possibility for populating doublet excited states (^{2}E and ^{2}T), while simultaneously preventing $^4T_2/^2E$ back intersystem crossing. As relaxation from these excited states to the $^4A_2$ ground state is spin forbidden, long-lived phosphorescence can be observed. However, Cr(III) species are often hampered by poor emissivity. Deoxygenated, deuterated solvents and deuteriation of ligands has been employed to help minimise quenching from non-radiative multiphonon relaxation pathways.[8]

In contrast to well-known precious metal lumophores, earth-abundant Cr(III) complexes of archetypal diimine ligands typically show Cr-centred phosphorescence in the 650–760 nm range. Related heteroleptic complexes provide some rational tuning of emission within similar wavelength ranges.[9]

Scheme 1 describes some important luminescent Cr(III) complexes, most of which have been reported in the last few years. Consideration of the N–Cr–N bite angles of the coordinated ligands is key. Thus, larger six-membered chelate rings are well suited in optimizing N–Cr–N bite angles towards 90° and this in turn reduces non-radiative deactivation.[7] Recent studies have clearly demonstrated the use of ligands such as *N*,*N*′-dimethyl-*N*-*N*′-dipyridine-2-yl-pyridine-2,6-diamine (ddpd),[10] 2,6-bis(2-pyridylmethyl)pyridine (bpmp),[11] and 1,1,1-tris(pyrid-2-yl)ethane (tpe)[12] that yield Cr(III) complexes with more intense emission properties and longer lifetimes.

During our current studies, Wenger, Piguet and co-workers described the first report of a Cr(III) complex with emission in the near-IR-II region (*ca.* 1067 nm) using ligand fields that combine optimised octahedral geometries with both σ- and π-donor/π-acceptor characteristics that potentially increase metal–ligand covalency.[13] This was achieved using a 3,6-di-*tert*-butyl-1,8-di(-pyridine-2-yl)-carbazole (dpc) ligand (Scheme 1) which imparts *trans* N–Cr–N bond angles of around 174° for $[Cr(dpc)_2]^+$. Excitation at 450 nm yielded an emission peaking at 1067 nm (with dual lifetimes of 1.4 and 6.3 μs) assigned to a possible admixture of ^{2}LMCT/^{2}E excited states. Unfortunately, the complex was only emissive at 77 K in a frozen matrix suggesting that further advances are necessary to identify near-IR luminescent Cr(III) species with broader potential applicability and utility.

We now report the development of luminescent Cr(III) complexes using 1,3-bis(2′-pyridylimino)-isoindoline (**bpi**) derivatives as terdentate N^N^N ligands.

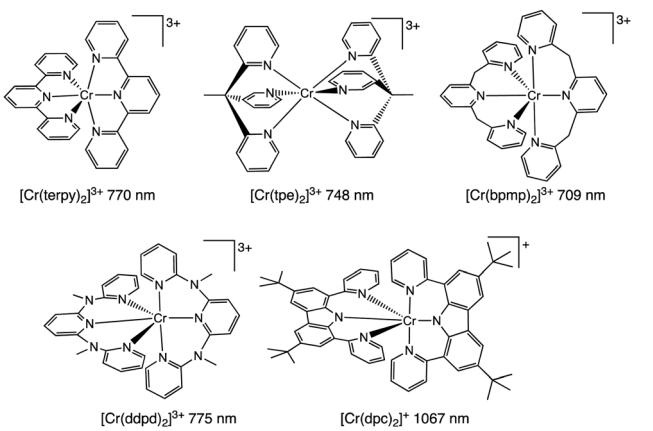

Scheme 1 Molecular structures of emissive Cr(III) complexes (with indicative luminescence wavelengths) using terdentate (N^N^N) ligands.

[a] School of Chemistry, Main Building, Cardiff University, Cardiff CF10 3AT, Cymru/Wales, UK. E-mail: Richardse10@cardiff.ac.uk, popesj@cardiff.ac.uk
[b] UK National Crystallographic Service, Chemistry, Faculty of Natural and Environmental Sciences, University of Southampton, Highfield, Southampton, SO17 1BJ, England, UK

† Electronic supplementary information (ESI) available: Experimental, additional spectra and DFT details. CCDC 2155916. For ESI and crystallographic data in CIF or other electronic format see DOI: https://doi.org/10.1039/d2cc01434c

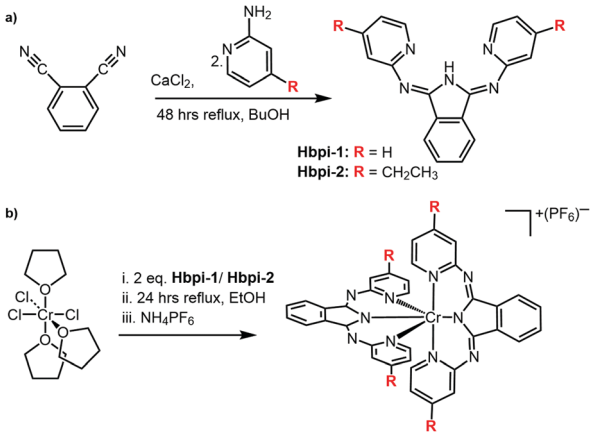

Scheme 2 (a) The synthetic route towards **Hbpi** ligands, and (b) coordination of the ligands to the Cr(III) centre. Full reagents and conditions are detailed in the ESI.†

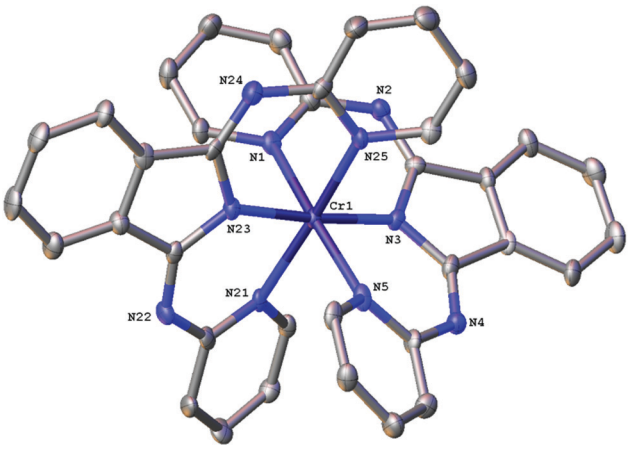

Fig. 1 X-Ray structure of $[Cr(\mathbf{bpi\text{-}1})_2]PF_6$. (H atoms, the counter ion and solvent molecules are omitted for clarity, ellipsoids are shown at 50% probability level.) Selected bond lengths (Å) and angles (°): N1–Cr 2.097(6), N5–Cr 2.088(6), N3–Cr 1.993(6), N21–Cr 2.107(6), N25–Cr 2.098(6), N23–Cr 1.986(6); N1–Cr–N5 172.8(2), N3–Cr–N23 175.6(2), N21–Cr–N25 173.5(2), N1–Cr–N3 86.2(2), N1–Cr–N21 92.1(2), N1–Cr–N23 91.0(2), N1–Cr–N25 90.4(2), N5–Cr–N3 87.4(2), N5–Cr–N21 85.3(2), N5–Cr–N23 95.6(2), N5–Cr–N25 92.9(2).

The two **Hbpi** pro-ligands (Scheme 2) were synthesized in a similar manner to previous reports on closely related complexes.[14] Reaction of the phthalonitrile reagent with a 2-aminopyridine species in the presence of $CaCl_2$ resulted[15] in the formation of the **Hbpi** ligands (see ESI† for details and characterisation data).

For the coordination chemistry, *mer*-$CrCl_3(THF)_3$ was reacted with two equivalents of ligand in EtOH to yield $[Cr(\mathbf{bpi})_2]PF_6$ (see ESI† for details). The complexes were purified using HPLC (using a water/MeCN solvent gradient) and corresponding high resolution mass spectra were obtained for both complexes (Fig. S1, ESI†) confirming the proposed formulation where each ligand is deprotonated and thus the complexes are monocationic.

Single, red needle crystals of $[Cr(\mathbf{bpi\text{-}1})_2]PF_6$ suitable for X-ray diffraction[16] were obtained from slow evaporation of a 1 : 1 : 1 diethyl ether/toluene/acetonitrile solution of complex (Table S1, ESI†) over 7 days. The structure revealed the complex crystallised as the diethyl ether solvate.

The bond angles that describe the coordination sphere can have a fundamental influence upon the photophysics of Cr(III): the N–Cr–N bite angles reveal the extent of distortion away from O_h geometry. For $[Cr(\mathbf{bpi\text{-}1})_2]PF_6$ the structure (Fig. 1) shows three *trans* N–Cr–N angles of 172.8(2)°, 175.6(2)° and 173.5(2)° (average = 174.0°). The average Cr–N bond length is 2.0615 Å with the $Cr–N_{(isoindoline)}$ bonds giving the two shortest distances. In comparison the N–Cr–N angles for $[Cr(dpc)_2]PF_6$ are 173.69(8)°, 173.66(7)°, 173.16(7)°, which are clearly comparable, and the Cr–N bond lengths also show a similar trend and average value. Therefore the **bpi-1** ligand imparts (Tables S2 and S3 ESI†) a favourable geometry at Cr(III).

To probe the electronic properties, a series of X-band EPR spectra were recorded for the complexes as frozen solutions in MeCN (140 K) and revealed broad signals at ~340 mT ($g \sim 2$), confirming the paramagnetic nature of the high-spin $S = 3/2$ centre of the ground state Cr^{3+} ($3d^3$) cation. Due to the poor resolution of the frozen solution spectra, both $[Cr(\mathbf{bpi\text{-}1})_2]PF_6$ and $[Cr(\mathbf{bpi\text{-}2})_2]PF_6$ were prepared as 1% doped solids in the corresponding $[Co(\mathbf{bpi})_2]PF_6$ matrix, a methodology previously indicated by Di Bilio *et al.*[17] to have good success in characterisation of Cr(III) systems and commonly utilised in EPR studies of first-row transition metal complexes.[18,19] This approach resulted in some improvements although the spectra are still complicated by some anisotropy within the material, presumably arising from uptake of the dopant cation in several sites within the host cobalt matrix (see Fig. 2; the cobalt matrices yielded no resolvable signals in their EPR spectra, confirming the diamagnetic nature of the host lattice). The Cr(III) spectra can be fully described by the spin Hamiltonian parameters for

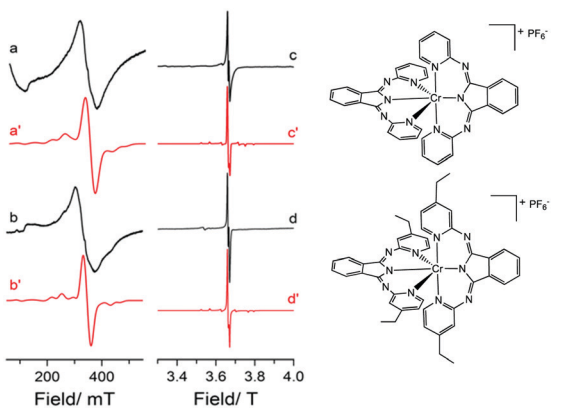

Fig. 2 Experimental and simulated EPR spectra of (a and c) $[Cr(\mathbf{bpi\text{-}1})_2]PF_6$ and (b and d) $[Cr(\mathbf{bpi\text{-}2})_2]PF_6$ recorded as 1% doped solids in their corresponding diamagnetic cobalt matrix. Experimental data were recorded at (a and b) X-band frequency, 140 K, and (c and d) W-band frequency, 20 K.

$S > 1/2$ systems:

$$\mathcal{H} = \mu_B\left(g_z H_z S_z + g_y H_y S_y + g_x H_x S_x\right) + D\left[\left\{S_z^2 - \frac{1}{3}S(S+1)\right\} + \left(\frac{E}{D}\right)\left(S_x^2 - S_y^2\right)\right]$$

where S is the total electron spin state, and D and E are the axial and rhombic zero-field splitting (ZFS) parameters. As the high-spin systems studied herein are dominated by zero-field splitting and are in the weak field limit (*i.e.*, $D \gg h\nu$) at 9.5 GHz, a series of W-band EPR (94 GHz) measurements were performed to ensure that the microwave quantum was greater than the magnitude of the zero-field splitting and facilitate accurate determination of the *g*-factor and ZFS parameters (Fig. 2). Resolution of the W-band spectra are improved, in particular for determination of the **g**-tensor, however strain effects broaden the low intensity fine structure components leading to challenges in accurate determination of the ZFS parameters. Hence, interpretation of the experimental spin Hamiltonian, listed in Table S4 (ESI†), is restricted to relative orders of magnitude and reference to other Cr(III) systems reported in the literature. The *D*-frames for both complexes were approximated as fully coincident with the molecular frame in the simulations, as often assumed for six-coordinate Cr(III) systems,[20] and as evidenced by the DFT calculated Euler angles from the fully relaxed geometry optimised ground-state structures (see Fig. S2, ESI†).

The small negative shift from $g_e \approx 2.0023$ for the two complexes is to be expected as a result of the less than half-filled d-orbitals, and the relatively small spin–orbit coupling parameter of the central chromium ion (ζCr^{3+} = 275 cm^{-1}).[21] The experimentally determined ZFS parameters (Table S4, ESI†) are noticeably smaller than other mononuclear Cr(III) complexes for which D is typically <0.6 cm^{-1}. This is justified (see Table S2) given that a purely cubic field would lead to $D = 0$.[22] Furthermore, there is good agreement with the complex $[CrLCl_3]$ that displays similar geometry, incorporating a tridentate ligand (**L** = (4′-2-pyridyl)-2,2′:6′,2″-terpyridine; similar Cr–N bond lengths) and a π-donor (Cl^-) in the axial coordinate site (known to increase the value of D; see ESI†).[23]

The redox characteristics of $[Cr(\textbf{bpi-1})_2]PF_6$ and $[Cr(\textbf{bpi-2})_2]PF_6$ were obtained through cyclic voltammetry. Firstly, the resultant voltammograms (Fig. S5, ESI†) did not show any features in the oxidative cathodic region. This is in general agreement with previous reports[24] on the redox features of Cr(III) complexes, including $[Cr(ddpd)_2]^{3+}$, but Wenger and co-workers report a reversible feature for $[Cr(dpc)_2]^+$ *ca.* +0.46 V *vs.* $Fc^{0/+}$ which was ascribed to a $Cr^{3+/4+}$ redox couple.[13] Polypyridyl Cr(III) complexes such as $[Cr(bipy)_2]^{3+}$ (ref. 25) and $[Cr(terpy)_2]^{3+}$ (ref. 26) are well known to show many ligand-based, reversible reductions.[27] For $[Cr(\textbf{bpi-1})_2]PF_6$ we observed four reversible or quasi-reversible features in the anodic window ($E_{1/2}$ at −0.55, −1.19, −1.49 and −1.72 V) which are mainly assigned to ligand-based processes. The voltammogram for $[Cr(\textbf{bpi-2})_2]PF_6$ was slightly different with reversible and irreversible features at −0.75, −1.05 and −1.38 V suggesting poorer electrochemical stability. It was notable that the first reversible reduction was subtly shifted to a more negative potential *versus* $[Cr(\textbf{bpi-1})_2]PF_6$ and thus consistent with a ligand-based process. The second, irreversible, feature at around −1.05 V may therefore be due to the $Cr^{3+/2+}$ couple as noted in both $[Cr(ddpd)_2]^{3+}$ and $[Cr(dpc)_2]^+$ *ca.* −1.1 V.

The UV-vis absorption properties of the complexes were ascertained using MeCN solutions. For reference, the ligands (Fig. S6, ESI†) absorb similarly between *ca.* 250–425 nm which is attributed to the different π → π* transitions ($>10\,000$ M^{-1} cm^{-1}) within the aromatic units. At 10^{-5} M the spectra of the complexes reveal features that are attributable to different ligand-based transitions ($\varepsilon > 5000$ M^{-1} cm^{-1}), with overlapping spin-allowed charge transfer bands also likely to contribute (supported by DFT, Fig. S7, ESI†). A moderately intense band at 450–525 nm is ascribed to an intraligand charge transfer (ILCT) arising from the amido donor of the isoindoline moiety and the conjugated iminopyridine groups; the subtle hypsochromic shift observed for ethyl-functionalised $[Cr(\textbf{bpi-2})_2]PF_6$ is consistent with this assignment. These absorption features and the tail of the ILCT band appear to obscure the spin-allowed ($^4A_2 \rightarrow {}^4T_2$, $^4A_2 \rightarrow {}^4T_1(F)$, $^4A_2 \rightarrow {}^4T_1(P)$) d–d transitions expected for Cr(III). At higher concentrations and longer wavelengths both complexes displayed a band *ca.* 750 nm (~ 10 M^{-1} cm^{-1}) and another even weaker feature ~850 nm. It is likely that one of these bands is due to the spin forbidden transition $^4A_2 \rightarrow {}^2E/{}^2T_1$. Previous work on related $[Cr(dpc)_2]^+$ has proposed, through computational studies, that a ^{2}LMCT band may also contribute in this region.[13]

For the luminescence studies, the complexes were prepared in MeCN and excited using 430 nm irradiation. As shown in Fig. 3, room temperature emission spectra were obtained under ambient, aerated sample conditions. $[Cr(\textbf{bpi-1})_2]PF_6$ has a main feature at approximately 950 nm with a shoulder to lower energy *ca.* 1050 nm with a tail extending to 1200 nm; the peak *ca.* 1270 nm is assigned to the $^1\Delta_g \rightarrow {}^3\Sigma_g^-$ transition of oxygen. In a frozen matrix (77 K, MeCN) the emission maximum is hypsochromically shifted by ~20 nm, the shoulder is somewhat more pronounced and photogeneration of $^1O_2$ is inhibited. For $[Cr(\textbf{bpi-2})_2]PF_6$ a relative hypsochromic shift in

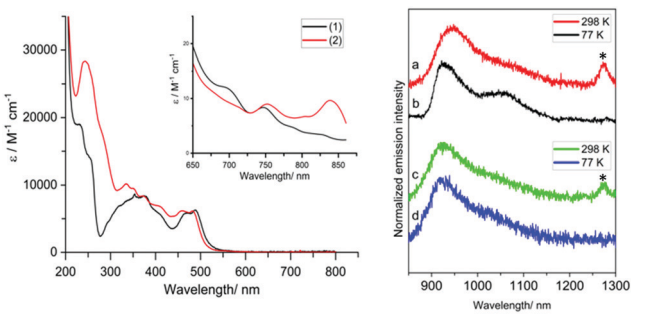

Fig. 3 Left: UV-vis absorption data for $[Cr(\textbf{bpi-1})_2]PF_6$ (1) and $[Cr(\textbf{bpi-2})_2]PF_6$ (2) including expansion of the long wavelength region. Emission data (λ_{ex} = 430 nm; 850 nm cut-on longpass filter) for $[Cr(\textbf{bpi-1})_2]PF_6$ (red, black) and $[Cr(\textbf{bpi-2})_2]PF_6$ (green, blue) recorded in MeCN. $^1\Delta_g \rightarrow {}^3\Sigma_g^-$ emission of oxygen highlighted by an asterisk.

Table 1 Absorption and emission data for the complexes recorded in MeCN

Complex	λ_{abs} (nm)	λ_{em}[a] (nm)	τ_{obs}[c] (μs)
$[Cr(\mathbf{bpi\text{-}1})_2]PF_6$	234, 256, 293 sh, 320 sh, 354 sh, 380, 412 sh, 464, 490, 607, 699, 750, 825 sh	948 (930)[b]	4.5 (8.0)[d]
$[Cr(\mathbf{bpi\text{-}2})_2]PF_6$	242, 282 sh, 335, 353, 377, 411 sh, 459, 483, 752, 840	929 (924)[b]	8.1 (25.0)[d]

[a] λ_{ex} = 430 nm. [b] Values in parenthesis recorded at 77 K. [c] λ_{ex} = 355 nm. [d] Values in parentheses recorded in deoxygenated solvent.

emission maximum was observed at λ_{em} = 929 nm (Table 1), which is attributed to the effect of the ethyl substituents and modulation of the ligand field strength at Cr(III).

The lifetimes of the emitting complexes were measured under aerated and degassed conditions (Table 1). In all cases the kinetic traces were fitted (Fig. S8, ESI†) to a single exponential decay yielding lifetimes in the μs domain under ambient conditions, which extended to around 8 μs and 25 μs, for $[Cr(\mathbf{bpi\text{-}1})_2]PF_6$ and $[Cr(\mathbf{bpi\text{-}2})_2]PF_6$ respectively, when deoxygenated, implying that oxygen acts as a quencher of these species. These lifetimes are consistent with a phosphorescent emission, which is likely to contain significant spin forbidden $^2E \rightarrow {}^4A_2$ character. The longer lifetime noted for $[Cr(\mathbf{bpi\text{-}2})_2]PF_6$ is consistent with the ligand-induced blue-shift in the emission maximum. Despite appearing in the near-IR range, the deoxygenated lifetimes for $[Cr(\mathbf{bpi})_2]PF_6$ are significantly longer than for $[Cr(terpy)_2]^{3+}$ (0.14 μs, de-aerated MeCN),[24] and $[Cr(dpc)_2]^+$ (see earlier discussion), but appear an order(s) of magnitude shorter than species such as $[Cr(ddpd)_2]^{3+}$ (898 μs, de-aerated H_2O) and $[Cr(tpe)_2]^{3+}$ (2800 μs, de-aerated $H_2O/HClO_4$) both of which emit *ca.* 750 nm.

The near-IR photophysical properties of $[Cr(\mathbf{bpi})_2]PF_6$ also invite comparison with Yb(III) species which display Yb(III)-centred luminescence at 980 nm (also typically with μs lifetimes) (Fig. S9, ESI†). However, unlike Yb(III), where the emission wavelength is generally insensitive to the ligand environment, the case of $[Cr(\mathbf{bpi\text{-}2})_2]PF_6$ demonstrates that substituents on the pyridyl donors can modulate and thus tune Cr-centred emission. This paves the way for future ligand iterations allowing the rational tuning of the Cr(III) emission within the attractive near-IR window. Further, the promising emission properties under oxygenated conditions at room temperature (and without recourse to deuterated solvents or ligands) imply that a range of applications could be considered for these complexes, including bioimaging and energy upconversion studies.

We thank Cardiff University and EPSRC (EP/R513003/1) for funding.

Conflicts of interest

There are no conflicts to declare.

Notes and references

1 L. A. Büldt and O. S. Wenger, *Chem. Sci.*, 2017, **8**, 7359.
2 L. A. Büldt and O. S. Wenger, *Dalton Trans.*, 2017, **46**, 15175.
3 L. S. Förster, *Chem. Rev.*, 1990, **90**, 331.
4 K. De Armond and L. S. Förster, *J. Chem. Phys.*, 1961, **55**, 2193.
5 J.-R. Jimenez, B. Doistau, M. Poncet and C. Piguet, *Coord. Chem. Rev.*, 2021, **434**, 213750.
6 P. A. Scattergood, *Organomet. Chem.*, 2021, **43**, 1.
7 S. Otto, M. Dorn, C. Förster, M. Bauer, M. Seitz and K. Heinze, *Coord. Chem. Rev.*, 2018, **359**, 102.
8 J.-C. Bünzli and C. Piguet, *Chem. Soc. Rev.*, 2005, **34**, 1048; A. J. Amoroso and S. J. A. Pope, *Chem. Soc. Rev.*, 2015, **44**, 4723.
9 B. Doistau, G. Collet, E. A. Bolomey, V. Sadat-Noorbakhsh, C. Besnard and C. Piguet, *Inorg. Chem.*, 2018, **57**, 14362; J.-R. Jimenez, B. Doistau, C. Besnard and C. Piguet, *Chem. Commun.*, 2018, **54**, 13228; J.-R. Jimenez, M. Poncet, B. Doistau, C. Besnard and C. Piguet, *Dalton Trans.*, 2020, **49**, 13528.
10 S. Otto, M. Grabolle, C. Förster, C. Kreitner, U. Resch-Genger and K. Heinze, *Angew. Chem., Int. Ed.*, 2015, **54**, 11572.
11 F. Reichenauer, C. Wang, C. Förster, P. Boden, N. Ugur, R. Baez-Cruz, J. Kalmbach, L. M. Carrella, E. Rentschler, C. Ramanan, G. Niedner-Schatteburg, M. Gerhards, M. Seitz, U. Resch-Genger and K. Heinze, *J. Am. Chem. Soc.*, 2021, **143**, 11843.
12 S. Treiling, C. Wang, C. Förster, F. Reichenauer, J. Kalmbach, P. Boden, J. P. Harris, L. Carrella, E. Rentschler, U. Resch-Genger, C. Reber, M. Seitz, M. Gerhards and K. Heinze, *Angew. Chem., Int. Ed.*, 2019, **58**, 18075.
13 N. Sinha, J.-R. Jimenez, B. Pfund, A. Prescimone, C. Piguet and O. S. Wenger, *Angew. Chem., Int. Ed.*, 2021, **133**, 2.
14 K.-N. T. Tseng, J. W. Kampf and N. K. Szymczak, *Organometallics*, 2013, **32**, 2046; E. Balogh-Hergovich, G. Speier, M. Reglier, M. Giorgi, E. Kuzmann and A. Vertes, *Inorg. Chem. Commun.*, 2005, **8**, 457.
15 W. O. J. Siegl, *Org. Chem.*, 1977, **42**, 1872.
16 S. J. Coles and P. A. Gale, *Chem. Sci.*, 2012, **3**, 683.
17 R. P. Bonomo and A. J. Di Bilio, *Chem. Phys.*, 1991, **151**, 323.
18 R. S. Drago, *Physical Methods for Chemists*, Surfside Scientific Publishers, Florida, USA, 2nd edn, 1992.
19 B. R. McGarvey, *J. Chem. Phys.*, 1964, **40**, 809.
20 J. Telser and J. Braz, *Chem. Soc.*, 2006, **17**, 1501.
21 G. M. Cole Jr. and B. B. Garrett, *Inorg. Chem.*, 1970, **9**, 1898.
22 J. M. López Plá, A. K. Boudalis, J. Telser and R. G. Raptis, *Inorg. Chim. Acta*, 2020, **502**, 119299.
23 T. Goswami and A. Misra, *J. Phys. Chem. A*, 2012, **116**, 5207.
24 J. C. Barbour, A. J. I. Kim, E. deVries, S. E. Shaner and B. M. Lovaasen, *Inorg. Chem.*, 2017, **56**, 8212.
25 Y. Sato and N. Tanaka, *Bull. Chem. Soc. Jpn.*, 1969, **42**, 1021; M. C. Hughes, J. M. Rao and D. J. Macero, *Inorg. Chim. Acta*, 1979, **35**, L321.
26 M. C. Hughes and D. J. Macero, *Inorg. Chem.*, 1976, **15**, 2040.
27 C. C. Scarborough, K. M. Lancaster, S. DeBeer, T. Weyhermuller, S. Sproules and K. Wieghardt, *Inorg. Chem.*, 2012, **51**, 3718.

